BSAR SIGNAL MODELING AND SLC IMAGE RECONSTRUCTION

T.P. Kostadinov, A.D. Lazarov
Institute of Information and Communication Technologies, Bulgarian Academy of Sciences, G. Bonchev 2, Sofia, Bulgaria,
Dept. of Informatics and Technical Sciences Burgas Free University, San Stefano 63 Burgas, Bulgaria
kostadinov.todor@yahoo.com, lazarov@bfu.bg

Keywords: BSAR, SLC, signal model, kinematics.

Abstract: In this paper, a Bistatic Synthetic Aperture Radar (BSAR) signal model and Single Look Complex (SLC) image obtained by multiple satellite BSAR system are considered. Geometry and kinematics of BSAR scenario, including a BSAR satellite transmitter and multiple receivers as well as a complicated surface of observation are described. BSAR signal model based on linear frequency modulated emitted waveform and BSAR scenario is derived. Standard Fourier transformation is applied to extract an SLC BSAR image of high quality on range and cross range directions. To verify the BSAR signal model and image extraction procedure a numerical experiment is carried out.

1 INTRODUCTION

In recent years raise in the interest of Bistatic Synthetic Aperture Radar (BSAR) technology is a fact. BSAR concept in SAR for Earth observation and BSAR spaceborne performance are analyzed in (Moccia A., 2002). Application of a BSAR method increases the quality of imaging and improves the functionality of the imaging radars (Moccia, A., 2005). Bistatic configurations of synthetic aperture radar imaging systems have been investigated in (Loffeld, O., 2003). New bistatic SAR techniques for imaging are proposed in (Ender, J. H. G, 2004). The problems of the focusing of SAR image are considered in (D'Aria, D., 2004). Passive space-surface bistatic SAR for local area monitoring is described in (Cherniakov M., 2009). Maritime target cross section estimation for an ultra-wideband forward scatter radar network is considered in (Daniel L., 2008). Results of a space-surface bistatic SAR image formation algorithm are presented in (Antoniou M., 2007).

BSAR in essence is a bistatic configuration, with a moving satellite transmitter, and two or more stationary receivers, spatially separated by a base line. The scene of observation includes stationary and/or moving objects. In latter case the system is referred to Generalized Bistatic Inverse Synthetic Aperture Radar (BISAR).

In the present work a scenario with satellite transmitter two receivers and stationary object is discussed. All components of bistatic SAR configuration are described in one and the same coordinate system. First, an accent is made on definition and implementation of BSAR geometry and kinematical vector equations. Second, a special attention is dedicated to processes of BSAR signal formation and image reconstruction procedure that comprises range and azimuth compressions implemented by Fourier transforms.

The rest of the paper is organized as follows. In Section 2 BSAR scenario that comprises geometry and kinematical equations of satellite transmitter carrier is described. In Section 4 a linear frequency waveform and BSAR signal model in topology with one satellite transmitter and two receivers are discussed in details. In Section 4 an image reconstruction algorithm is derived. In Section 5 results of a numerical experiment are graphically illustrated and thoroughly discussed. In Section 6 conclusions are made.

Kostadinov T. and Lazarov A.
BSAR SIGNAL MODELING AND SLC IMAGE RECONSTRUCTION.
DOI: 10.5220/0005414000650071
In *Proceedings of the First International Conference on Telecommunications and Remote Sensing (ICTRS 2012)*, pages 65-71
ISBN: 978-989-8565-28-0
Copyright © 2012 by SCITEPRESS – Science and Technology Publications, Lda. All rights reserved

2 BSAR GEOMETRY

Three dimensional (3-D) BSAR scenario presented in Fig. 1 comprises satellite transmitter described by current position vector $\mathbf{R}^s(p)$ in discrete time instant *p*, stationary receivers described by current position vectors $\mathbf{R}_1^r$ and $\mathbf{R}_2^r$, and a target of interest, all situated in Cartesian coordinate system *Oxyz*. The target is presented as an assembly of point scatterers in the same Cartesian coordinate system as the transmitter and the receivers.

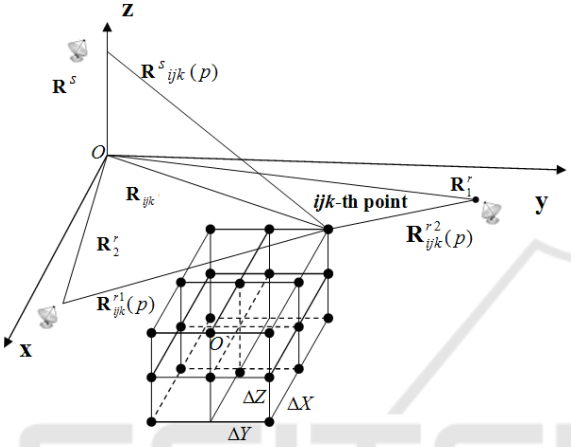

Figure 1: 3-D geometry of BSAR scenario

Denote $\mathbf{R}^s{}_{ijk}(p) = \left[x_{ijk}(p), y_{ijk}(p), z_{ijk}(p)\right]^T$ as a range distance vector measured from the satellite transmitter with the current vector position $\mathbf{R}^s(p)$ to the *ijk*th point scatterer of the object space at the moment *p*, is described by the vector equation

$$\mathbf{R}^s{}_{ijk}(p) = \mathbf{R}^s(p) + \mathbf{V}\left(\frac{N}{2} - p\right)T_p + \mathbf{R}_{ijk} \qquad (1)$$

where $\mathbf{V}$ is the satellite's vector-velocity, T_p is the pulse repetition period, *N* is the number of emitted pulses

$$\mathbf{R}_{ijk} = [x_{ijk}, y_{ijk}, z_{ijk}]^T \qquad (2)$$

is the position vector of the target.
Range distance vector between the *ijk*th point scatterer and the first receiver is defined by:

$$\mathbf{R}^{r1}{}_{ijk} = \mathbf{R}_1^r - \mathbf{R}_{ijk} \qquad (3)$$

Range distance vector between *ijk*th point scatterer and the second receiver is defined by:

$$\mathbf{R}^{r2}{}_{ijk} = \mathbf{R}_2^r - \mathbf{R}_{ijk} \qquad (4)$$

Round trip distance transmitter-*ijk*th point scatterer-first receiver expressed as

$$R^1{}_{ijk}(p) = \left|\mathbf{R}^s{}_{ijk}(p)\right| + \left|\mathbf{R}^{r1}{}_{ijk}\right|. \qquad (5)$$

Round trip distance transmitter-*ijk*th point scatterer-second receiver expressed as

$$R^2{}_{ijk}(p) = \left|\mathbf{R}^s{}_{ijk}(p)\right| + \left|\mathbf{R}^{r1}{}_{ijk}\right|. \qquad (6)$$

3 LFM PULSES AND BSAR SIGNAL MODEL

The satellite transmitter transmits a series of electromagnetic waves to the moving target, which are described analytically by sequence of *N* linear frequency modulated pulses each of which is described by

$$\dot{S}(t) = \mathbf{rect}\frac{t}{T}\mathbf{exp}\left\{-j\left[\omega t + bt^2\right]\right\}, \qquad (7)$$

where $\omega = 2\pi\frac{c}{\lambda}$ is the angular frequency; $c = 3.10^8$ m/s is the speed of the light; λ is the wavelength of the signal; *T* is the time duration of a LFM pulse; $b = \frac{2\pi\Delta F}{T}$ is the LFM rate. The bandwidth of the transmitted pulse provides the dimension of the range resolution cell.
The deterministic component of the BSAR signal, reflected by *ijk*th point scatterer of the target and registered by first and second receiver can be described by the expression (Lazarov A., 2011)

$$\dot{S}^{1,2}_{ijk}(p,t) = a_{ijk}\mathbf{rect}\frac{t - t^{1,2}_{ijk}(p)}{T} \times \times \mathbf{exp}\left\{-j\left[\begin{array}{l}\omega\left(t - t^{1,2}_{ijk}(p)\right) + \\ + b\left(t - t^{1,2}_{ijk}(p)\right)^2\end{array}\right]\right\} \qquad (8)$$

where

$$\mathbf{rect}\frac{t-t_{ijk}^{1,2}(p)}{T}=\begin{cases}1, 0\le\dfrac{t-t_{ijk}^{1,2}(p)}{T}<1,\\ 0, \dfrac{t-t_{ijk}^{1,2}(p)}{T}<0\\ 0, \dfrac{t-t_{ijk}^{1,2}(p)}{T}\ge 1\end{cases} \quad (9)$$

where a_{ijk} is the reflection coefficient of the *ijk*th point scatterer, a 3-D image function; $t_{ijk}^{1,2}(p)=\dfrac{R_{ijk}^{1,2}(p)}{c}$ is the time delay of the signal from the *ijk*th point scatterer; t is the time dwell or the fast time of the BSAR signal which in discrete form can be written as

$$t=[k_{ijk\,\min}^{1,2}(p)+k-1]\Delta T \quad (10)$$

where $k=\overline{1,[k_{ijk\,i\max}^{1,2}(p)-k_{ijk\,\min}^{1,2}(p)]+K}$ is the sample number of a LFM pulse; $K=\dfrac{T}{\Delta T}$ is the full number of samples of the LFM pulse, ΔT is the time duration of a LFM sample, $k_{ijk\,\min}^{1,2}(p)=\left\lceil\dfrac{t_{ijk\,\min}^{1,2}(p)}{\Delta T}\right\rceil$ is the number of the radar range bin where the signal, reflected by the nearest point scatterer of the target is detected, $t_{ijk\,\min}^{1,2}(p)=\dfrac{R_{ijk\,\min}^{1,2}(p)}{c}$ is the minimal time delay of the BSAR signal reflected from the nearest point scatterer of the target

$K(p)=k_{ijk\,\max}^{1,2}(p)-k_{ijk\,\min}^{1,2}(p)$ is the relative time dimension of the target;

$k_{ijk\,\max}^{1,2}(p)=\left\lceil\dfrac{t_{ijk\,\max}^{1,2}(p)}{\Delta T}\right\rceil$ is the number of the radar range bin where the signal, reflected by farthest point scatterer of the target is detected; $t_{ijk\,\max}^{1,2}(p)=\dfrac{R_{ijk\,\max}^{1,2}(p)}{c}$ is the maximum round trip time delay of the BSAR signal reflected from the farthest point scatterer of the target and received in both receivers.

The range vector coordinates from the satellite transmitter to the *ijk*-th point scatterer can be calculated by the following equations

$$\begin{aligned}x^{s}{}_{ijk}(p)&=x_s-V_xT_p[(N/2)-p]-x_{ijk},\\ y^{s}{}_{ijk}(p)&=y_s-V_yT_p[(N/2)-p]-y_{ijk},\\ z^{s}{}_{ijk}(p)&=z_{0s}-V_zT_p[(N/2)-p]-z_{ijk}\end{aligned} \quad (11)$$

The distance from satellite transmitter to the *ijk*th point scatterer is defined by

$$R_{ijk}^{s}(p)=\left[\left(x_{ijk}^{s}(p)\right)^2+\left(y_{ijk}^{s}(p)\right)^2+\left(z_{ijk}^{s}(p)\right)^2\right]^{\frac{1}{2}} \quad (12)$$

The range vector - coordinates from the *ijk*-th point scatterer to the receivers can be calculated by the following equations

$$\begin{aligned}x_{ijk}^{1,2}&=x_r^{1,2}-x_{ijk},\\ y_{ijk}^{1,2}&=y_r^{1,2}-y_{ijk},\\ z_{ijk}^{1,2}&=z_r^{1,2}-z_{ijk}\end{aligned} \quad (13)$$

The distance from *ijk*th point scatterer to the receivers is defined by

$$R_{ijk}^{1,2}=\left[\left(x_{ijk}^{1,2}\right)^2+\left(y_{ijk}^{1,2}\right)^2+\left(z_{ijk}^{1,2}\right)^2\right]^{\frac{1}{2}} \quad (14)$$

The deterministic components of the BSAR signal return from the target and registered in first and second receivers are defined as a superposition of signals reflected by point scatterers placed on the target, i.e.

$$\begin{aligned}\dot{S}^{1,2}(p,t)&=\sum_{ijk}\dot{S}_{ijk}^{1,2}(p,t)\\ &=\sum_{ijk}\left(\begin{array}{l}a_{ijk}\mathbf{rect}\dfrac{t-t_{ijk}^{1,2}(p)}{T}\times\\ \times\mathbf{exp}\left\{-j\left[\begin{array}{l}\omega\left(t-t_{ijk}^{1,2}(p)\right)+\\ +b\left(t-t_{ijk}^{1,2}(p)\right)^2\end{array}\right]\right\}\end{array}\right)\end{aligned} \quad (15)$$

SCITEPRESS SCIENCE AND TECHNOLOGY PUBLICATIONS

which in discrete form can be written as

$$\begin{aligned}\dot{S}^{1,2}(p,t) &= \sum_{ijk}\dot{S}^{1,2}_{ijk}(p,t)\\ &= \sum_{ijk}a_{ijk}\mathbf{rect}\frac{(k^{1,2}_{ijk\,\min}(p)+k)\Delta T - t^{1,2}_{ijk}(p)}{T}\\ &\times\mathbf{exp}\left\{-j\left[\begin{array}{l}\omega\left((k^{1,2}_{ijk\,\min}(p)+k)\Delta T\right)-t^{1,2}_{ijk}(p)\big)+\\ +b\left((k^{1,2}_{ijk\,\min}(p)+k)\Delta T\right)-t^{1,2}_{ijk}(p)\big)^2\end{array}\right]\right\}\end{aligned} \tag{16}$$

where

$$\begin{aligned}&\mathbf{rect}\frac{(k^{1,2}_{ijk\,\min}(p)+k)\Delta T - t^{1,2}_{ijk}(p)}{T}\\ &=\begin{cases}1 \text{ if } 0\le\dfrac{(k^{1,2}_{ijk\,\min}(p)+k)\Delta T - t^{1,2}_{ijk}(p)}{T}<1\\ 0 \text{ if } \dfrac{(k^{1,2}_{ijk\,\min}(p)+k)\Delta T - t^{1,2}_{ijk}(p)}{T}<0\\ 0 \text{ if } \dfrac{(k^{1,2}_{ijk\,\min}(p)+k)\Delta T - t^{1,2}_{ijk}(p)}{T}\ge 1\end{cases}\end{aligned} \tag{17}$$

where $k=0,[k^{1,2}_{ijk\,\max}(p)-k^{1,2}_{ijk\,\min}(p)]+K-1$.

For programming implementation all terms, including image function a_{ijk}, rectangular function

$$\mathbf{rect}\frac{(k^{1,2}_{ijk\,\min}(p)+k)\Delta T - t^{1,2}_{ijk}(p)}{T} \tag{18}$$

and exponential function

$$\mathbf{exp}\left\{-j\left[\begin{array}{l}\omega\left((k^{1,2}_{ijk\,\min}(p)+k)\Delta T\right)-t^{1,2}_{ijk}(p)\big)+\\ +b\left((k^{1,2}_{ijk\,\min}(p)+k)\Delta T\right)-t^{1,2}_{ijk}(p)\big)^2\end{array}\right]\right\} \tag{19}$$

are presented as multidimensional matrices to which entry-wise product is applied.

Demodulation (dechirping) of the BSAR signal return is performed by multiplication with a complex conjugated emitted waveform, i.e.

$$\begin{aligned}\hat{S}^{1,2}(t,p) &= S(t,p)\times\mathbf{rect}\frac{t}{T}\exp\left[-j(\omega t+bt^2\right]\\ &= \sum_{ijk}a_{ijk}\mathbf{rect}\frac{t-t^{1,2}_{ijk}(p)}{T}\times\\ &\exp\left\{j\left[\begin{array}{l}\omega\left(t-t^{1,2}_{ijk}(p)\right)+\\ +b.\left(t-t^{1,2}_{ijk}(p)\right)^2\end{array}\right]\right\}.\exp\left[-j(\omega t+bt^2\right]\end{aligned} \tag{20}$$

which yields

$$\begin{aligned}\hat{S}^{1,2}(t,p) &= \sum_{ijk}a_{ijk}\mathbf{rect}\frac{t-t^{1,2}_{ijk}(p)}{T}\\ &\times\exp\left\{-j\left[(\omega+2bt)t^{1,2}_{ijk}(p)-b\left(t^{1,2}_{ijk}\right)^2(p)\right]\right\}\end{aligned} \tag{21}$$

Denote the current angular frequency of emitted LFM pulse as $\omega(t)=\omega+2bt$, where ω is the carrier angular frequency, and b is the chirp rate, $t=k\Delta T$ is the discrete time parameter, where k is the sample number, ΔT is the sample time duration. Then the current discrete frequency can be written as $\omega_k=\omega+2b(k\Delta T)$ or $\omega_k=k\left(\frac{\omega}{k}+2b(\Delta T)\right)=k\Delta\omega_k$.

Then expression (24) can be rewritten as (Lazarov A., 2011)

$$\begin{aligned}\hat{S}^{1,2}(t,p) &= \sum_{ijk}a_{ijk}\mathbf{rect}\frac{t-t^{1,2}_{ijk}(p)}{T}\\ &\times\exp\left[-j\left(2\omega(t)\frac{R^{1,2}_{ijk}(p)}{c}-b\left(\frac{2R^{1,2}_{ijk}(p)}{c}\right)^2\right)\right]\end{aligned} \tag{22}$$

which in discrete form can be written as

$$\begin{aligned}\hat{S}^{1,2}(k,p) &= \sum_{ijk}a_{ijk}\mathbf{rect}\frac{(k^{1,2}_{ijk\,\min}(p)+k)\Delta T - t^{1,2}_{ijk}(p)}{T}\\ &\times\exp\left[-j\left(2\omega_k\frac{R^{1,2}_{ijk}(p)}{c}-b\left(\frac{2R^{1,2}_{ijk}(p)}{c}\right)^2\right)\right]\end{aligned} \tag{23}$$

The expression (23) can be interpreted as a projection of the three-dimensional image function a_{ijk} onto two-dimensional BSAR signal plane

SCITEPRESS
SCIENCE AND TECHNOLOGY PUBLICATIONS

$\hat{S}^{1,2}(k,p)$ by the projective operator, the exponential term

$$\exp\left[-j\left(2\omega_k\frac{R_{ijk}^{1,2}(p)}{c}-b\left(\frac{2R_{ijk}^{1,2}(p)}{c}\right)^2\right)\right] \quad (24)$$

Then the 2-D mage function, $a_{ijk}^{1,2}$ can be extracted from 2-D BSAR signal in two receivers by the inverse operation

$$a_{ijk}^{1,2}=\sum_{p=1}^{N}\sum_{k=1}^{K}\hat{S}^{1,2}(k,p).\exp\left[j\left(2\omega_k\frac{R_{ijk}^{1,2}(p)}{c}-b\left(\frac{2R_{ijk}^{1,2}(p)}{c}\right)^2\right)\right] \quad (25)$$

where k is the discrete coordinate measured onto the line of sight of the object's geometric centre, p is the azimuth discrete coordinate.

4 IMAGE RECONSTRUCTION ALGORITHM

First order Taylor expansion of the exponential term

$$\exp\left[j\left(2\omega_k\frac{R_{ijk}^{1,2}(p)}{c}-b\left(\frac{2R_{ijk}^{1,2}(p)}{c}\right)^2\right)\right] \quad (26)$$

and its substitution in (23) yields the following image extraction procedure

$$a_{ijk}^{1,2}(\hat{p},\hat{k})=\sum_{p=1}^{N}\left[\sum_{k=1}^{K}\left(\hat{S}^{1,2}(p,k).\exp\left(j2\pi\frac{k\hat{k}}{K}\right)\right)\right].\exp\left(j2\pi\frac{p\hat{p}}{N}\right). \quad (27)$$

Range compression

$$\tilde{S}^{1,2}(p,\hat{k})=\frac{1}{K}\sum_{k=1}^{K}\hat{S}^{1,2}(p,k).\exp\left(j2\pi\frac{k\hat{k}}{K}\right) \quad (28)$$

Azimuth compression

$$a_{ijk}^{1,2}(\hat{p},\hat{k})=\frac{1}{N}\sum_{p=1}^{N}\tilde{S}^{1,2}(p,\hat{k}).\exp\left(j2\pi\frac{p\hat{p}}{N}\right) \quad (29)$$

where $\hat{p}=\overline{1,N}$ and $\hat{k}=\overline{1,K}$ are ijkth point scatterer's azimuth and range discrete coordinates, respectively.

Range and azimuth (cross range) compressions are implemented by standard fast Fourier transforms.

5 NUMERICAL EXPERIMENT

To prove the properties of the 3-D SAR signal model with linear frequency modulation and to verify the correctness of the BSAR image reconstruction procedures including 2-D FFT range compression and azimuth compression a numerical experiment is carried out. It is assumed that the geometry of the target and the movement of the radar system are depicted in a 3-D Cartesian coordinate system of observation $Oxyz$. Vector coordinates of the initial point scatterer are as follow $x_{ijk}^0=0$ m, $y_{ijk}^0=0$ m, $z_{ijk}^0=0$ m; The target object of interest is a six storage building and has the following dimensions – height 15m, width 120m, dept 55 m; The satellite initial coordinates are: $x_s=-8{,}5$ km, $y_s=1{,}2$ km, $z_{0s}=200$ km; the satellite velocities are $V_x=V_y=1404$ m/s $V_z=0$ m/s, vector-coordinates of the firs receiver are: $x_1^r=2{,}5$ km, $y_1^r=1{,}2$ km, $z_1^r=300$ m; vector-coordinates of the second receiver are: $x_2^r=2{,}5$ km, $y_2^r=2{,}2$ km, $z_2^r=300$ m. The distance between the first receiver and the second one is a 1000 m on y direction. This distance is called base line. The BSAR pulse parameters: the wavelength is $\lambda=3.10^{-2}$ m; the time duration of the LFM pulse $T=10^{-6}$ s; the pulse repetition period $T_p=5.10^{-3}$ s; the carrier frequency $f=10$ GHz; the frequency bandwidth of the LFM pulse $\Delta F=3.10^8$ Hz; the number of emitted pulses N = 512, the number of samples of LFM pulse K = 256. The mathematical expectation of the normalized intensities of the point scatterers placed on the ship target is $a_{ijk}=0.01$.

Experimental results are presented in the following figures. In Figs. 2 and 7 a demodulated BSAR signal with real and imaginary parts, measured in first and second receiver, respectively, are depicted. In Figs. 3 and 8 range compressed BSAR signal with real and imaginary parts, measured in first and second receiver, respectively, are depicted. In Figs. 4 and 9 azimuth compressed BSAR signal with real and imaginary parts, measured in first and second receiver, respectively, are depicted. In Figs. 5 and 10 frequency azimuth compressed BSAR signal with real and imaginary parts, measured in first and second receiver, respectively, are depicted. In Figs. 6 and 11 single look complex images are presented with a module (*a*) and phase (b) of the images obtained in first and second receiver, respectively.

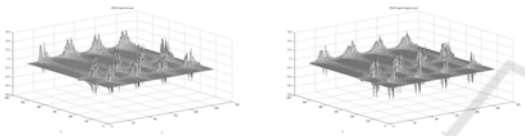

(*a*) (*b*)

Figure 2: Demodulated BSAR signal: real part (*a*), imaginary part (*b*) in first receiver.

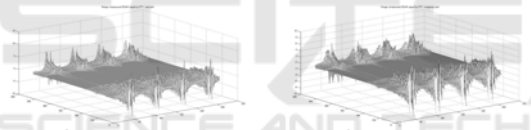

(*a*) (*b*)

Figure 3: Range compressed BSAR signal: real part (*a*), imaginary part (*b*) in first receiver.

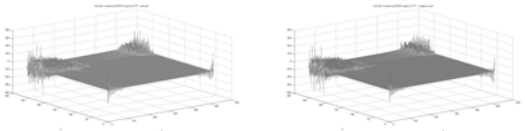

(a) (b)

Figure 4: Azimut compressed BSAR signal: real part(*a*), imaginary part (*b*).

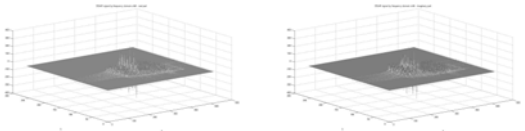

(a) (b)

Figure 5: Frequency shifted azimut compressed BSAR signal: real part (*a*), imaginary part (*b*).

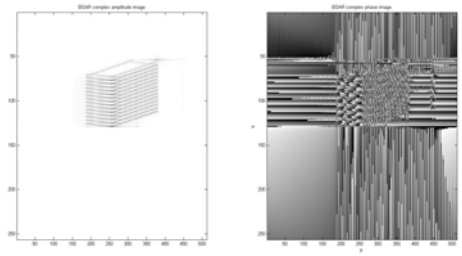

(*a*) (*b*)

Figure 6: Single looks complex image in the first receiver: module (a), phase (b).

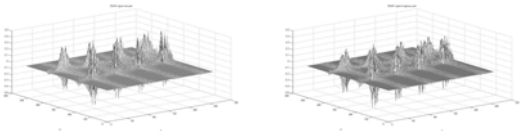

(*a*) (*b*)

Figure 7: Demodulated BSAR signal: real part (*a*), imaginary part (*b*) in second receiver.

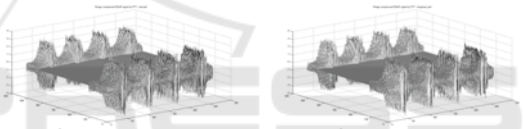

(*a*) (*b*)

Figure 8: Range compressed BSAR signal: real part (*a*), imaginary part (*b*) in second receiver.

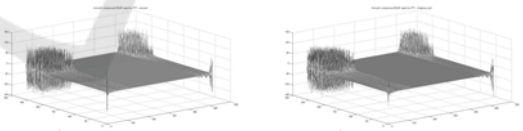

(*a*) (*b*)

Figure 9: Azimuth compressed BSAR signal: real part (*a*), imaginary part (*b*) in second receiver.

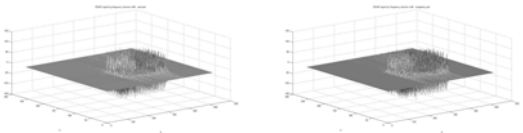

(*a*) (*b*)

Figure 10: Frequency shifted azimuth compressed focused BSAR signal: real part (*a*), imaginary part (*b*).

SCITEPRESS SCIENCE AND TECHNOLOGY PUBLICATIONS

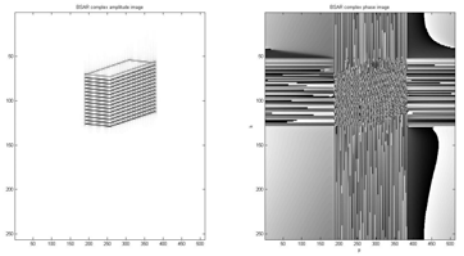

(*a*) (*b*)

Figure 11: Single looks complex image in the second receiver: module (*a*), phase (*b*).

The comparison analysis of two single look complex images illustrates the functionality of the geometry, kinematics and signal models in BSAR scenario with multiple receivers. Between the two SLC images there are differences in the module and phase due to the baseline between the receivers. The phase difference in SLC images can be used to generate a complex interferogram that can be applied for three dimensional measurements of the observed object.

6 CONCLUSION

In the present work BSAR approach of signal formation and image reconstruction has been used. Mathematical expressions to determine the range distance to a particular point scatterer from the object space have been derived. The model of the BSAR signal return based on a linear frequency modulated transmitted signal, 3-D geometry and reflectivity properties of point scatterers from the object space has been described. The mathematical expression of BSAR target image – six storage building has been derived. Based on the concept of BSAR signal formation a classical image reconstruction procedure including range compression and azimuth compression implemented by Fourier transformation has been analytically derived. To verify the three dimensional BSAR geometry and kinematics, signal model, algorithms and image reconstruction, a numerical experiment has been carried out and results have been graphically illustrated. The multiple receiver BSAR geometry and kinematics, equations of LFM BSAR signal model can be used for modelling of signal formation process and to test image reconstruction procedures.

ACKNOWLEDGEMENTS

This work is supported by Project NATO ESP.EAP.CLG. 983876 and Project DDVU 02/50/2010.

REFERENCES

Moccia A., Rufmo, G., D'Errico, M., Alberti G., et. al. 2002. BISSAT: A bistatic SAR for Earth observation, In *International Geoscience and Remote Sensing Symposium (IGARSS'02*), Vol. 5, June 24-28, 2002, pp. 2628-2630.

Moccia, A., Salzillo, G., D'Errico, M., Rufino, G., Alberti, G. 2005. Performace of bistatic synthetic aperture radar. In *IEEE Trans. on AES*, vol. 41, No. 4 2005, pp. 1383 – 1395

Loffeld, O., Nies, H., Peters, V., and Knedlik, S. 2003.Models and useful relations for bistatic SAR processing", In *International Geoscience and Remote Sensing Symposium* (IGARSS), vol. 3, Toulouse, France, July 21—25, pp. 1442—1445.

Ender, J. H. G., Walterscheid, I., and Brenner, A. R. 2004. New aspects of bistatic SAR: Processing and experiments." In *International Geoscience and Remote Sensing Symposium* (IGARSS), vol. 3, Anchorage, AK, Sept. 20—24, pp. 1758—1762.

D'Aria, D., Guarnieri, A. M., and Rocca, F. 2004. Focusing bistatic synthetic aperture radar using dip move out. *IEEE Transactions on Geoscience and Remote Sensing*, 42, no. 7, pp. 1362—1376.

Lazarov A., Kabakchiev Ch., Rohling H., Kostadinov T. 2011. Bistatic Generalized ISAR Concept with GPS Waveform. In *2011 IRS - Leipzig*, pp. 849-854.

Lazarov A., Kabakchiev Ch., Cherniakov M., Gashinova M., Kostadinov T. 2011. Ultra Wideband Bistatic Forward Scattering Inverse Synthetic Aperture Radar Imaging. In *2011 IRS - Leipzig*, pp. 91-96.

Cherniakov M., Plakidis E., Antoniou M., Zuo R. 2009. Passive Space-Surface Bistatic SAR for Local Area, Monitoring: Primary Feasibility Study, In *2009 EuMA*, 30 September - 2 October 2009, Rome, Italy

Daniel L., Gashinova M., Cherniakov M.. 2008. Maritime Target Cross Section Estimation for an Ultra-Wideband Forward Scatter Radar Network. In *2008 EuMA*, Amsterdam, pp. 316-319.

Antoniou M., Saini R., Cherniakov M. 2007. Results of a Space-Surface bistatic SAR image formation algorithm, In *IEEE Trans. GRS*, vol. 45, no. 11, pp. 3359-3371.